J. Fluid Mech. (1978), *vol.* 89, *part* 3, *pp.* 497–514
Printed in Great Britain

The motion of a large gas bubble rising through liquid flowing in a tube

By R. COLLINS,
Department of Mechanical Engineering, University College London

F. F. DE MORAES,† J. F. DAVIDSON AND D. HARRISON
Department of Chemical Engineering, University of Cambridge

(Received 30 September 1977 and in revised form 12 June 1978)

The theory presented here describes the motion of a large gas bubble rising through upward-flowing liquid in a tube. The basis of the theory is that the liquid motion round the bubble is inviscid, with an initial distribution of vorticity which depends on the velocity profile in the liquid above the bubble. Approximate solutions are given for both laminar and turbulent velocity profiles and have the form

$$U_s = U_c + (gD)^{\frac{1}{2}}\,\phi(U_c/(gD)^{\frac{1}{2}}), \tag{1}$$

U_s being the bubble velocity, U_c the liquid velocity at the tube axis, g the acceleration due to gravity, and D the tube diameter; ϕ indicates a functional relationship the form of which depends upon the shape of the velocity profile. With a turbulent velocity profile, a good approximation to (1) which is suitable for many practical purposes is

$$U_s = U_c + U_{s0}, \tag{2}$$

U_{s0} being the bubble velocity in stagnant liquid. Published data for turbulent flow are known to agree with (2), so that in this case the theory supports a well-known empirical result. Our laminar flow experiments confirm the validity of (1) for low liquid velocities.

1. Introduction

When a large volume of gas is introduced at the lower end of a long vertical tube filled with stagnant liquid, the gas forms an axisymmetric bullet-shaped bubble which is known as a slug. The velocity U_s of a slug rising steadily in stagnant liquid is a function of g, the acceleration due to gravity, D, the tube diameter, and μ, ρ and σ, which are respectively the viscosity, density and surface tension of the liquid. From dimensional analysis it follows that the Froude number $Fr = U_s/(gD)^{\frac{1}{2}}$ is a unique function of $N_f = g^{\frac{1}{4}}D^{\frac{3}{4}}\rho/\mu$ and $M = g\mu^4/\rho\sigma^3$. For a sufficiently large tube diameter it might be expected that the slug velocity would be independent of liquid properties and experiments do show that there is a regime in which Fr is independent of N_f and M. This inertia-controlled regime specified by $N_f > 300$ and $Eo = N_f^{\frac{4}{3}}M^{\frac{1}{3}} > 100$, where Eo is the Eötvos number (White & Beardmore 1962; Wallis 1969), is the subject of the present paper in which previous analysis for the stagnant-liquid problem is extended

† Present address: Department of Chemical Engineering, University of Maringá, Caixa postal 331, 87.100 Maringá, Brazil.

to include the effect of liquid flow on the slug velocity. The topic has important industrial applications and has been studied by a number of investigators, for example Behringer (1936), Griffith & Wallis (1961), Nicklin, Wilkes & Davidson (1962), Zuber & Findlay (1965) and Nicolitsas & Murgatroyd (1968).

Our purpose is primarily to give a theory describing the effect of liquid motion in the tube on the slug velocity and shape. The liquid velocity profile far above the rising slug is particularly important: most of the published data are for turbulent velocity profiles, partly because this is the most important case industrially; to get a wider variety of profiles we carried out experiments with laminar motion above the rising slug.

Previous workers correlated data using an equation of the form

$$U_s = C_1 \bar{U} + C_2 (gD)^{\frac{1}{2}}, \tag{1.1}$$

the essential idea behind which is to isolate the effect of the mean upward liquid velocity $\bar{U}$ from that of the other variables; C_1 and C_2 are coefficients. Nicklin *et al.* (1962) deduced that, with turbulent liquid flow, C_1 is very close to $U_c/\bar{U}$, where U_c is the maximum (centre-line) velocity in the flowing liquid; thus an alternative to (1.1) is

$$U_s = U_c + C_2 (gD)^{\frac{1}{2}}, \tag{1.2}$$

and it was suggested that $C_2 = 0{\cdot}35$, as for a slug rising in stagnant liquid (Stewart & Davidson 1967).

Slight differences in the values of C_1 and C_2 given by various authors led Nobel (1972) to doubt whether the forms of (1.1) and (1.2) are appropriate; in particular the relation between C_1 and $U_c/\bar{U}$ was questioned. He proposed more complicated equations without, however, considering the detailed dynamics of the flow.

Our theory, for both laminar and turbulent liquid flow, can be summarized by writing

$$U_s = U_c + (gD)^{\frac{1}{2}} \phi(U_c/(gD)^{\frac{1}{2}}), \tag{1.3}$$

where ϕ indicates a functional relationship. The theory thus provides strong support for the deduction by Nicklin *et al.* (1962) for turbulent liquid flow leading to (1.2). By comparing (1.3) with (1.1), C_1 and C_2 are predicted. The theory also shows that there are circumstances in which the linearized result (1.2) is an acceptable substitute for the full solution (1.3), and (1.2) with $C_2 = 0{\cdot}35$ is a good approximation for many practical cases. There is excellent agreement of turbulent theories with experimental data. For laminar flow, comparison between theory and experiment is more difficult, but our experimental data are in reasonable agreement with predictions.

2. Theory

We argue that the flow relative to the slug rising in a moving liquid can be treated as that of an inviscid liquid possessing vorticity. Such analysis develops that of Dumitrescu (1943) and Layzer (1955), who assumed irrotational motion round a slug rising in stagnant liquid. The neglect of viscosity in analysing these flows can be justified by considering the convection and diffusion of the vorticity generated by the motion of the slug. Figure 1 shows the motion as seen (*a*) by a fixed observer, and (*b*) an observer moving with the slug. This motion may be compared with that due

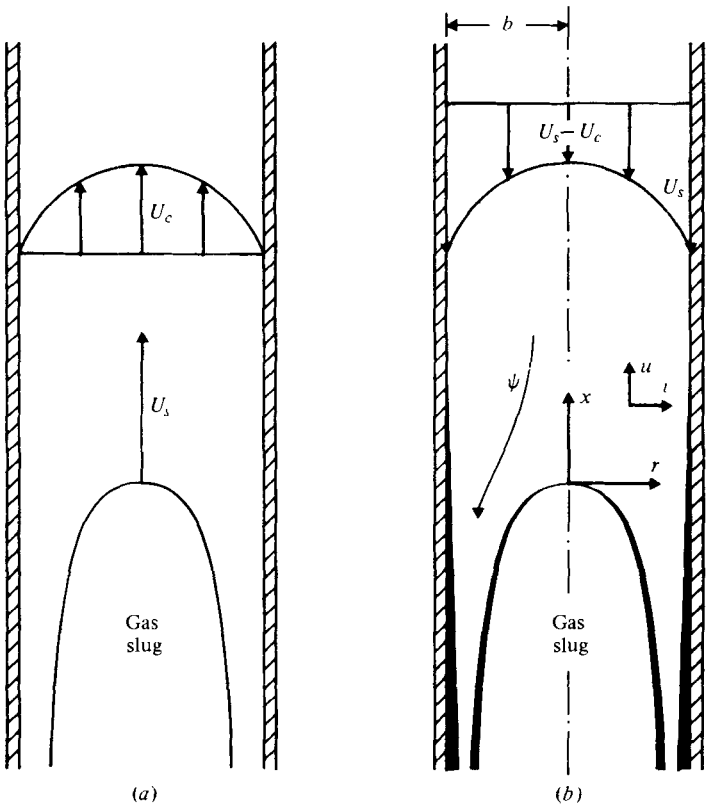

FIGURE 1. Gas slug rising in flowing liquid: (*a*) as seen by a fixed observer; (*b*) as seen by an observer moving with the slug. The thickening lines indicate developing boundary layers.

to a slug rising in stagnant liquid. The fundamental difference between the two cases is that for the motion in figure 1 there is a relative movement between the liquid and the tube wall far upstream of the slug and this relative movement generates the velocity profile, which can be regarded as a boundary layer filling the tube. The velocity profile remains unchanged until the liquid approaches the slug nose, where there are two fresh sources of vorticity provided by the free surface and by the change in relative motion between liquid and wall.

The boundary layers arising from these sources are indicated with exaggerated thickness in figure 1(*b*). Both layers will be thin provided the slug Reynolds number $Re_s = \rho U_s D/\mu$ is high, and we observe from §1 that in the inertia-controlled regime in a stagnant liquid $Re_s = Fr\, N_f > 0{\cdot}35 \times 300 = 105$. The growth of these layers is inhibited by the acceleration of the liquid round the slug nose, which also prevents separation.

Because these boundary layers are thin, the pressure distribution can be well represented by an irrotational flow when the slug rises in stagnant liquid (Dumitrescu 1943; Layzer 1955; Collins 1968). When the slug rises in flowing liquid, the pressure distribution can likewise be represented by a rotational flow which possesses a prescribed distribution of vorticity upstream. In the latter case, the idea is that the primary effect of viscosity is to generate the initial velocity profile far upstream and

that the subsequent motion is that of an inviscid liquid with initial vorticity. The theoretical basis for such an investigation is well established (Lamb 1932; Batchelor 1967), and there is a history of successful applications in other fields, for example in analysing flows in the blade rows of axial compressors and turbines (Hawthorne 1967).

For axisymmetrical motion we use cylindrical co-ordinates (x, r, θ) with the origin located at the slug nose as indicated in figure 1(*b*). It is more convenient to develop the analysis using the tube radius b rather than the diameter D. In terms of Stokes's stream function ψ, the local velocity components u and v in the x and r directions are given by $ru = -\partial\psi/\partial r$ and $rv = \partial\psi/\partial x$. Lamb (1932, p. 245) shows that for steady motion

$$\frac{\partial^2\psi}{\partial x^2}+\frac{\partial^2\psi}{\partial r^2}-\frac{1}{r}\frac{\partial\psi}{\partial r} = r^2 f(\psi). \tag{2.1}$$

The function $f(\psi)$ is arbitrary and defines the vorticity distribution far upstream of the slug where ψ is independent of x. The exact solutions considered here correspond to $f(\psi) =$ constant and $f(\psi) = k(\psi + C)$, where k and C are constants.

In solving (2.1), the boundary conditions to be satisfied in all cases are:

(*a*) $\psi = 0$ on the slug surface, as yet undefined;

(*b*) $\psi =$ constant on the tube wall, where $\eta = r/b = 1$;

(*c*) far upstream of the slug ψ must be a given function of η, determined by the velocity profile in the liquid;

(*d*) the gas pressure in the slug is constant so the static pressure in the liquid must also be constant along the slug surface.

Bernoulli's equation in this rotational flow takes the form

$$p/\rho + \tfrac{1}{2}q^2 + gb\xi = p_0(\psi)/\rho,$$

where $q^2 = u^2 + v^2$, $\xi = x/b$ and p_0 is the stagnation pressure. Hence at the slug surface, (*d*) requires that

$$q^2 + 2gb\xi = 0. \tag{2.2}$$

Following the procedure employed for stagnant liquid (Dumitrescu 1943) and when the upstream liquid is rotating about the tube axis (Collins & Hoath 1973) the left-hand side of (2.2) is expanded in a Taylor series about the origin to give

$$q^2 + 2gb\xi = ((q^2 + 2gb\xi)_0'')\,\eta^2/2! + ((q^2 + 2gb\xi)_0^{\mathrm{iv}})\,\eta^4/4! + \ldots = 0. \tag{2.3}$$

Here primes denote derivatives with respect to η of a quantity evaluated at $\psi = 0$ and considered as a function of η only and the suffix 0 denotes evaluation at the origin. From symmetry q^2 and ξ are even functions of η and hence only derivatives of even order appear in the expansion. An exact solution to the free-boundary problem would make all coefficients zero in (2.3).

Results for stagnant liquids (Davies & Taylor 1950; Collins 1966; Batchelor 1967) show that the slug velocity is predicted with remarkable accuracy by using only the first term of (2.3), thus satisfying the boundary condition (*d*) near the stagnation point. This procedure will be followed here, when the liquid has vorticity, and we shall present single-term approximations satisfying only the first term of (2.3).

This term requires that $(u^2 + v^2)_0'' + 2gb\xi_0'' = 0$ and, since the origin of the co-ordinates is a stagnation point and the slug and liquid flow are symmetrical, then

$$u_0 = v_0 = u_0' = \xi_0' = 0.$$

Model	Section no.	Type of solution	Satisfaction of differential equation (2.1)	Satisfaction of free-surface boundary condition
A Laminar	4.1	Separation of variables, single term	Exact	Satisfies first term of (2.3); valid near apex
A Turbulent	5.1	Separation of variables, single term	Exact	Satisfies first term of (2.3); valid near apex
B Laminar	4.2	Dipole solution	Exact	As *A*, but valid over a larger region near apex
B Turbulent	5.2	Dipole solution	Approximate	As *A*, but valid over a larger region near apex

TABLE 1. Theoretical models.

It follows that

$$v_0' = (-gb\xi_0'')^{\frac{1}{2}} = (gb^2/a)^{\frac{1}{2}}, \tag{2.4}$$

where $a = -b/\xi_0''$ denotes the radius of curvature of the slug boundary at the stagnation point and an explicit expression for the slug velocity is obtained by rewriting (2.4) in the form

$$U_s - U_c = (gb)^{\frac{1}{2}}/[(a/b)^{\frac{1}{2}} v_0'/(U_s - U_c)]. \tag{2.5}$$

Equation (2.5), which, though derived from only the first term of (2.3), is exact, shows that the slug velocity may be deduced from two features of the flow at the stagnation point, namely

(i) the radius of curvature of the nose of the slug, represented by the dimensionless ratio a/b,

(ii) the velocity derivative at the stagnation point, represented by the dimensionless ratio $v_0'/(U_s - U_c)$.

The objective of the approximate model solutions considered here is to describe the geometry of the free surface as closely as possible so that a/b and $v_0'/(U_s - U_c)$ may be deduced from the models for use in (2.5).

Table 1 summarizes the results in this paper. Two types of solution of (2.1), designated models *A* and *B*, were obtained. Model *A* is based on separation of variables and uses the first term in a series for ψ, following the method of Layzer (1955). Model *B* uses the method of Collins (1967), which is based on a dipole solution with a disposable parameter chosen so as to match the flow near the slug nose with a one-dimensional model of the flow downstream. Models *A* and *B* both constitute first approximations in the sense that they eliminate only the first term in (2.3), but model *B* produces a smaller error in the pressure distribution because it describes the real slug geometry in the vicinity of the stagnation point more closely. In table 1, the adjectives 'laminar' and 'turbulent' indicate the form of velocity profile far upstream of the slug: 'laminar' implies a parabolic velocity profile, 'turbulent' a profile of logarithmic or similar form as found in pipes with steady flow at high Reynolds number.

3. Laminar profiles

If $f(\psi) = 2U_c/b^2$ in (2.1), then the vorticity distribution is linear in the flow far ahead of the bubble, so that the velocity profile there is of parabolic form. Exact solutions of (2.1) which are appropriate for problems in which the fluid is contained

within a tube and which will generate slug-like shapes (Lai 1964), are obtained by separation of variables, which gives

$$\psi = \tfrac{1}{2}U_s b^2\eta^2 - \tfrac{1}{2}U_c b^2\eta^2(1-\tfrac{1}{2}\eta^2) - (U_s - U_c)\sum_{i=1}^{\infty} \eta b^2 (d_i/k_i)\exp(-k_i\xi)J_1(k_i\eta). \quad (3.1)$$

In (3.1), k_i is the ith zero of the first-order Bessel function J_1 and the coefficients d_i require determination. The perturbation to the liquid flow which is represented by the series in (3.1) is in fact irrotational, and (3.1) differs from those solutions used by Layzer and Dumitrescu for a slug rising in stagnant liquid only in so far as it includes the rotational second term, which describes the velocity profile in the flowing liquid.

From (3.1), the velocity components are given by

$$u = -U_s + U_c(1-\eta^2) + (U_s - U_c)\sum_{i=1}^{\infty} d_i \exp(-k_i\xi)J_0(k_i\eta), \quad (3.2)$$

and

$$v = (U_s - U_c)\sum_{i=1}^{\infty} d_i \exp(-k_i\xi)J_1(k_i\eta). \quad (3.3)$$

Note from (3.2) that $u \to U_c(1-\eta^2) - U_s$ when $\xi \to +\infty$, confirming that the absolute velocity $u + U_s$ is parabolic far upstream. The origin of the co-ordinates is set at the stagnation point, so that

$$\sum_{i=1}^{\infty} d_i = 1. \quad (3.4)$$

The surface of the slug, which will correspond to the stream surface $\psi = 0$ in (3.1), then follows as

$$\eta = -\tfrac{1}{2}U_c\eta^3/(U_s - U_c) + 2\sum_{i=1}^{\infty} (d_i/k_i)\exp(-k_i\xi)J_1(k_i\eta), \quad (3.5)$$

from which the radius of curvature at the nose of the slug, denoted by a, may be shown to be given by

$$a/b = \left[4\sum_{i=1}^{\infty} d_i k_i\right] \Big/ \left[\sum_{i=1}^{\infty} d_i k_i^2 + 4U_c/(U_s - U_c)\right]. \quad (3.6)$$

For the present solution, representing the parabolic velocity profile, v is given by (3.3) and the radius of curvature by (3.6), so that (2.5), which relates the slug velocity to the geometry of the flow, gives

$$(U_s - U_c)^3 - gb(U_s - U_c)\left[\sum_{i=1}^{\infty} d_i k_i^2\right] \Big/ \left[\sum_{i=1}^{\infty} d_i k_i\right]^3 - 4gbU_c \Big/ \left[\sum_{i=1}^{\infty} d_i k_i\right]^3 = 0. \quad (3.7)$$

Only the positive real root of this cubic equation for $U_s - U_c$ is of interest here, giving

$$U_s = U_c + (gb)^{\frac{1}{2}} \frac{\left[\sum_{i=i}^{\infty} d_i k_i^2\right]^{\frac{1}{2}}}{\left[\sum_{i=1}^{\infty} d_i k_i\right]^{\frac{3}{2}}} \Phi\left\{\frac{2U_c}{(gb)^{\frac{1}{2}}}\left[\frac{3\sum_{i=1}^{\infty} d_i k_i}{\sum_{i=1}^{\infty} d_i k_i^2}\right]^{\frac{3}{2}}\right\}, \quad (3.8)$$

where

$$\Phi(s) = \begin{cases} (2/3^{\frac{1}{2}})\cos\tfrac{1}{3}\arccos s & \text{when } s \leqslant 1, \quad (3.9) \\ (2/3^{\frac{1}{2}})\cosh\tfrac{1}{3}\operatorname{arccosh} s & \text{when } s \geqslant 1. \quad (3.10) \end{cases}$$

Asymptotic expansions for $\Phi(s)$ for subsequent use are

$$\Phi(s) \sim \begin{cases} 1 + s/3^{\frac{3}{2}} + \ldots & \text{for} \quad s \ll 1, \qquad (3.11) \\ (2s/3^{\frac{3}{2}})^{\frac{1}{3}} + \frac{1}{3}(2s/3^{\frac{3}{2}})^{-\frac{1}{3}} + \ldots & \text{for} \quad s \gg 1. \qquad (3.12) \end{cases}$$

In principle, any desired number of the coefficients d_i may be evaluated and hence the slug shape and velocity determined to any level of approximation. Even for the stagnant-liquid problem, however, the complexity is such that no more than three terms have been found, eliminating the first two coefficients in (2.3) and producing a second approximation (Dumitrescu 1943). The present problem is further complicated since the coefficients d_i will in general be functions of $U_c/(gb)^{\frac{1}{2}}$; it may be concluded from this that the result in (3.8) has the general form

$$U_s = U_c + (gb)^{\frac{1}{2}} \phi(U_c/(gb)^{\frac{1}{2}}). \qquad (3.13)$$

We now consider approximate models of the flow.

4. Laminar model solutions

Theories developed for slugs and bubbles in stagnant liquids suggest that satisfactory descriptions of the flow can be obtained using only one term of the series solution (Layzer 1955; Davies & Taylor 1950), or a form of the series representing a single dipole (Collins 1967); laminar models *A* and *B* are based on these approaches.

4.1. *Laminar model A*

Model *A* contains only the first term in the series in (3.1) and hence, from (3.4), $d_1 = 1$. With this choice it is possible to produce only a first approximation in the sense defined in § 2, and from (3.8) we obtain

$$U_s = U_c + \frac{(gb)^{\frac{1}{2}}}{k_1^{\frac{1}{2}}} \Phi\left\{\frac{2U_c}{(gb)^{\frac{1}{2}}}\left(\frac{3}{k_1}\right)^{\frac{3}{2}}\right\}, \qquad (4.1)$$

where $k_1 = 3{\cdot}8317$ is the first zero of the Bessel function J_1. Although its definition may appear to make Φ an awkward entity the solution in (4.1) is in fact easily evaluated and in that sense it does not need simplification. Consider, nevertheless, the asymptotic behaviour of Φ for small values of its argument, i.e. for low values of $U_c/(gb)^{\frac{1}{2}}$. From (3.11) and (4.1)

$$U_s = U_c(1 + 2/k_1^2) + (gb/k_1)^{\frac{1}{2}} + \ldots = 1{\cdot}13U_c + 0{\cdot}511(gb)^{\frac{1}{2}} + \ldots, \qquad (4.2)$$

retaining only the lowest-order terms. Enhancement of the coefficient of U_c from its apparent value of unity in (4.1) will be observed. With a parabolic velocity profile, $\overline{U} = \frac{1}{2}U_c$, so that, in terms of the variables $\overline{U}$ and D, (4.2) becomes

$$U_s = 2{\cdot}27\overline{U} + 0{\cdot}361(gD)^{\frac{1}{2}} + \ldots \ . \qquad (4.3)$$

The coefficient 2·27 agrees remarkably, though fortuitously, with Wallis's (1969, p. 293) conjecture. The linearized form in (4.3) is in fact an excellent description of the full solution for a substantial range of the variable $\overline{U}/(gD)^{\frac{1}{2}}$.

With the liquid stagnant, (4.2) reproduces Layzer's result, $U_s/(gb)^{\frac{1}{2}} = 0{\cdot}511$, whereas experiments are usually regarded as confirming Dumitrescu's theoretical value of

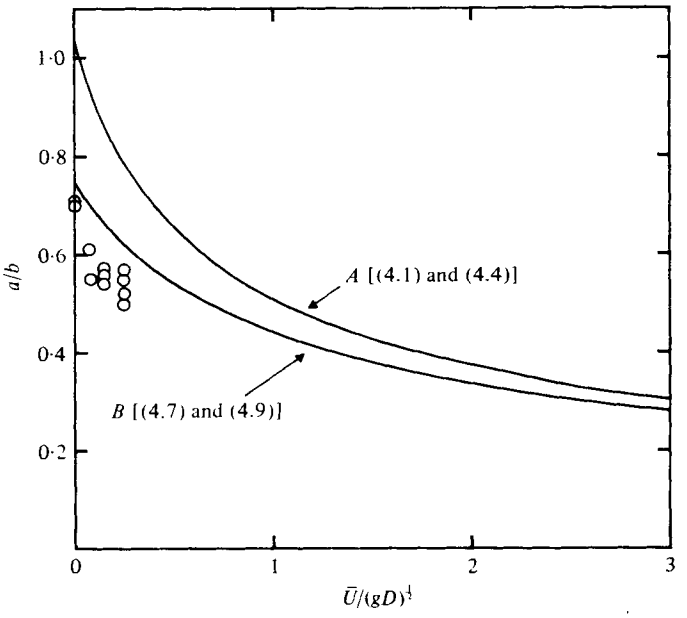

FIGURE 2. Variation of nose radius of curvature with liquid velocity for laminar models A and B. ○, experimental values, present work.

0·496 (Stewart & Davidson 1967). This slight deficiency of laminar model A may be attributed to its overestimating the radius of curvature at the stagnation point: the variation of a/b with $\bar{U}/(gD)^{\frac{1}{2}}$ is plotted in figure 2 by using, in conjunction with (4.1), the equation derived from (3.6),

$$a/b = 4k_1/(k_1^2 + 4U_c/(U_s - U_c)). \tag{4.4}$$

Figure 2 shows that the slug nose becomes more pointed as the flow velocity $\bar{U}$ increases.

4.2. *Laminar model B*

Dumitrescu's solution for the stagnant-liquid problem comprised a set of second approximations for an arbitrary range of nose radii from $a/b = 0{\cdot}5$ to $a/b = 0{\cdot}9$. A particular value for the nose radius, and hence the slug Froude number, was then selected from this set by requiring that the nose shape should merge smoothly with the downstream shape, which was determined from a simple one-dimensional view of the downstream flow. In studying wall effects for spherical-cap bubbles, Collins (1967) found that results almost identical with Dumitrescu's could be obtained rather more simply from an alternative form of first approximation and the extension of that work to the flowing-liquid problem forms model B. If we choose to write

$$d_i = \frac{k_i \exp(-k_i c)/J_0^2(k_i)}{\sum_{i=1}^{\infty} k_i \exp(-k_i c)/J_0^2(k_i)}, \tag{4.5}$$

then in the region $\xi > -c$ the irrotational perturbation to the flowing stream given

by the series in (3.1) may be shown to represent a dipole situated on the axis at the point $\xi = -c$ (cf. Collins 1967). For convenience, we define

$$T_{\alpha,1}(c) = \sum_{i=1}^{\infty} k_i^{\alpha-1} d_i, \tag{4.6}$$

$T_{\alpha,1}(c)$ being a particular case of the function $T_{\alpha,\beta}(c)$ given by Collins (1967). Using (4.5) and (4.6) we find from (3.6) that

$$a/b = 4T_{2,1}[T_{3,1} + 4U_c/(U_s - U_c)]^{-1}, \tag{4.7}$$

from (3.7) that

$$(U_s - U_c)^3 - gb(U_s - U_c)\, T_{3,1}/T_{2,1}^3 - 4gbU_c/T_{2,1}^3 = 0, \tag{4.8}$$

and from (3.8) that

$$U_s = U_c + (gb)^{\frac{1}{2}} \frac{T_{3,1}^{\frac{1}{2}}}{T_{2,1}^{\frac{3}{2}}} \Phi\left\{\frac{2U_c}{(gb)^{\frac{1}{2}}}\left(\frac{3T_{2,1}}{T_{3,1}}\right)^{\frac{3}{2}}\right\}. \tag{4.9}$$

The linearized form of (4.9) for small values of the argument of Φ is

$$U_s = U_c(1 + 2/T_{3,1}) + (gb)^{\frac{1}{2}} T_{3,1}^{\frac{1}{2}}/T_{2,1}^{\frac{3}{2}} + \dots\ . \tag{4.10}$$

Note from (4.5) and (4.6) that the asymptotic behaviour as $c \to \infty$ is $T_{\alpha,1} \to k_1^{\alpha-1}$, so that (4.9) and (4.10) then simply reproduce (4.1) and (4.2), thus yielding laminar model *A* from laminar model *B*. The effect of varying c is to change the radius of curvature at the nose and model *B* may be regarded as providing a set of first approximations for an arbitrary range of a/b from which, in the manner of Dumitrescu, we may select that solution which merges with a one-dimensional model of the shape downstream. The result, as in his analysis, is to select $a/b = 0{\cdot}75$ when $U_c = 0$, giving $c = 0{\cdot}8072$, $T_{3,1} = 25{\cdot}065$ and $T_{2,1} = 4{\cdot}6996$. The linearized form (4.10) then becomes

$$U_s = 1{\cdot}08U_c + 0{\cdot}491(gb)^{\frac{1}{2}} + \dots = 2{\cdot}16\overline{U} + 0{\cdot}347(gD)^{\frac{1}{2}} + \dots, \tag{4.11}$$

which gives an excellent description of the full solution: for example when

$$\overline{U}/(gD)^{\frac{1}{2}} = 2,$$

the value of U_s from (4.11) is about 4 % greater than that from (4.9). Figure 2 shows that model *B* gives an improved estimate of the nose radius of curvature: at $U_c = 0$ it reproduces an earlier theoretical result (Collins 1967); moreover the value $a/b = 0{\cdot}75$ at $U_c = 0$ is in good agreement with published experiments (Stewart & Davidson 1967) and, as indicated, agrees with our own experiments to be described in §6. Comparing models *A* and *B*, it is the improvement in the nose radius which gives the corresponding improvement in the coefficients between (4.3) and (4.11); however, the small changes in the coefficients show that they are insensitive to geometrical deficiencies in the models.

The full solution for laminar model *B* in (4.9) may be rewritten in terms of $\overline{U}$ and D to give

$$U_s = 2\overline{U} + 0{\cdot}347(gD)^{\frac{1}{2}}\, \Phi(2{\cdot}39\overline{U}/(gD)^{\frac{1}{2}}) \tag{4.12}$$

and (4.11) and (4.12) constitute the main results of the theory for the laminar profile. Comparison with results from new experiments will be discussed in §6, where it will be shown that the theory is confirmed for low values of $\overline{U}/(gD)^{\frac{1}{2}}$.

Finally, before considering the theory for turbulent profiles we recall that laminar

models A and B both provide only first approximations whereas Dumitrescu's model for a stagnant liquid gave a second approximation. One might consider constructing a second approximation for our problem by ignoring the dependence of d_i on $U_c/(gb)^{\frac{1}{2}}$, as we have effectively already done in model B, and simply using in (3.8) these values for d_1, d_2 and d_3 from Dumitrescu's analysis. These have been recalculated by Collins & Hoath (1973) and found to be $d_1 = 0{\cdot}8011$, $d_2 = 0{\cdot}1385$ and $d_3 = 0{\cdot}0604$. The results of that approach will not be cited, however, because they are virtually identical with those for model B. In any case, the effect of ignoring the dependence of d_i on $U_c/(gb)^{\frac{1}{2}}$ is to make this alternative a second approximation only when $U_c \equiv 0$. For finite flow rates it reverts to being a first approximation, as are models A and B.

5. Turbulent profiles

Frequently used relationships for the turbulent velocity distribution such as power laws, the universal profile, results from Prandtl's mixing-length theory and von Kármán's similarity hypothesis are unsuitable for the following analysis because they do not exhibit the zero velocity gradient on the tube axis which symmetry demands. Fortunately, equations due to Reichardt (1951) and Pai (1957) are satisfactory both in this respect and in their ability to describe experimental data, but their forms are such that they do not allow an exact analytical solution of (2.1). A simplified theory employing those profiles will be given in §5.2, but consideration is first given in §5.1 to results from a second exact solution of (2.1) which provides rather flatter profiles than does the laminar theory.

5.1. *Turbulent model A*

By separating the variables and transforming the resulting equation for the radial direction into Kummer's equation, it may be shown that an exact solution of (2.1) satisfying boundary conditions (*a*), (*b*) and (*c*) of §2 and with

$$f(\psi) = (\alpha^2/b^4)\{\psi + (b^2/\alpha)(U_s - U_c)\}$$

is $$\psi = (U_s - U_c)(b^2/\alpha)[\exp(\tfrac{1}{2}\alpha\eta^2) - \tfrac{1}{2}\alpha\eta^2 \exp(-\beta\xi - \tfrac{1}{2}\alpha\eta^2) M(1-\nu, 2, \alpha\eta^2) - 1], \quad (5.1)$$

where $\eta = r/b$, $\xi = x/b$, and $\beta(\alpha) = 2(\nu\alpha)^{\frac{1}{2}}$. $M(A, B, z)$ is the confluent hypergeometric function and $\nu = \nu(\alpha)$ is such that $M(1-\nu, 2, \alpha) = 0$, so that α is the smallest real positive zero of M. The parameter α determines the shapes of the upstream velocity profiles, whose forms, relative to a fixed observer, are given by

$$u = (U_c - U_w)[\exp(\tfrac{1}{2}\alpha) - \exp(\tfrac{1}{2}\alpha\eta^2)]/[\exp(\tfrac{1}{2}\alpha) - 1] + U_w, \quad (5.2)$$

where U_w is a slip velocity allowed at the wall of the tube. These profiles are flatter than the parabolic profile, which in fact corresponds to $\alpha = 0$, and they can be made to fit turbulent profiles reasonably well for small values of α, as shown in figure 3(*a*). Details of the solution are given by de Moraes (1977), who discusses also methods of assigning values to U_w by comparison with other turbulent profiles. Using (5.1) as a model to provide a first approximation in the sense defined in §2, it may be shown that from (2.5)

$$U_s = U_c + \beta^{-\frac{1}{2}}(1 + 2\alpha/\beta^2)^{\frac{1}{2}}(gb)^{\frac{1}{2}} \quad (5.3)$$

and $$U_c/(gb)^{\frac{1}{2}} = \beta^{-\frac{1}{2}}(1 + 2\alpha/\beta^2)^{\frac{1}{2}}\{[\exp(\tfrac{1}{2}\alpha) - 1]/\tfrac{1}{2}\alpha - 1\}/(1 - \overline{U}/U_c). \quad (5.4)$$

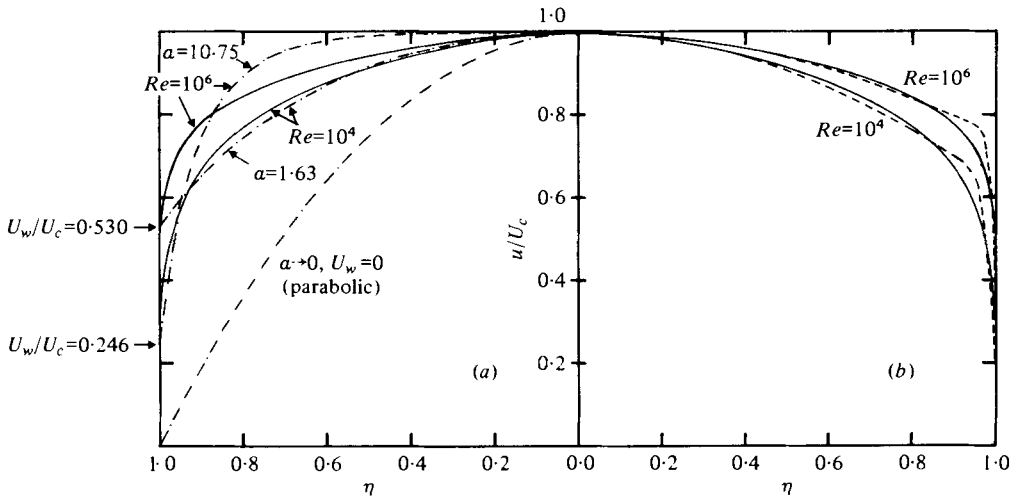

FIGURE 3. Velocity profiles. (*a*) –·–, turbulent model *A*: ——, Reichardt, (5.14). (*b*) ——, Reichardt, (5.14); – – –, Pai, (5.16).

For a given value of $\overline{U}/U_c$, (5.4) shows that α and $\beta(\alpha)$ are determined by $U_c/(gb)^{\frac{1}{2}}$. Hence (5.3) can be written in the same general form as (3.13) and is thus again in agreement with the conclusion of Nicklin *et al.* (1962) on the role played by the centre-line velocity U_c in determining the slug velocity. De Moraes (1977) has also shown that, for small values of α and $U_w = 0$, (5.3) reproduces (4.3), the result obtained for laminar model *A* with small values of $U_c/(gb)^{\frac{1}{2}}$, and, in the limit $\alpha \to 0$, it reproduces Layzer's result for the stagnant-liquid case.

The advantage of a model which constitutes an exact solution of (2.1) is that the convection of the free-stream vorticity around the slug is correctly described. Its disadvantage is that the resultant velocity profiles compare favourably with experimental data only for relatively small values of α, as shown in figure 3(*a*). Turbulent model *B*, on the other hand, represents the velocity profiles very well but at the cost of not satisfying (2.1) exactly.

5.2. *Turbulent model B*

Consider the following modification of (3.1):

$$\psi = \tfrac{1}{2}U_s b^2\eta^2 + \tfrac{1}{2}U_c b^2\eta^2 t(\eta) - (U_s - U_c)\psi^*. \tag{5.5}$$

In this equation, $t(\eta)$ describes the rotational part of the upstream flow and ψ^* represents the irrotational perturbation to that stream given by the infinite series in (3.1).

Clearly (5.5) does not satisfy (2.1) at all points in the flow, except when $t(\eta)$ describes a parabolic velocity profile, but it does describe a flow which has a prescribed distribution of upstream vorticity, is confined within a tube, has a stagnation point at the origin and moves around a slug-like shape. The motion represented by (5.5) is irrotational on the tube axis and in the immediate neighbourhood of the stagnation point, as any exact solution of (2.1) must be, but it is deficient in its description of the way in which the vorticity is convected around the slug. In using (5.5) the hope is that the result of the analysis may be as insensitive to that deficiency as are laminar models

A and B in respect of their deficiencies in slug geometry. Justification for this expectation is given in §5.2.1.

The velocity profile has maximum upward velocity U_c and zero velocity gradient on the tube axis, so that $t_0 = -1$ and $t_0' = 0$, the suffix 0 denoting evaluation on the axis. ψ^* will be taken to be the perturbation associated with a dipole as used in §4.2 for laminar model B.

From (5.5), the radius of curvature of the branch of the streamline $\psi = 0$ which forms the slug boundary may be shown to be given by

$$a/b = 4T_{2,1}/(T_{3,1} + 4t_0'' U_c/(U_s - U_c)), \tag{5.6}$$

and the cubic equation which arises for $U_s - U_c$ is then

$$(U_s - U_c)^3 - gb(U_s - U_c)\, T_{3,1}/T_{2,1}^3 - 4gbt_0'' U_c/T_{2,1}^3 = 0. \tag{5.7}$$

This cubic is similar to (4.8) and the solution, analogous to (4.9), is

$$U_s = U_c + (gb)^{\frac{1}{2}} \frac{T_{3,1}^{\frac{1}{2}}}{T_{2,1}^{\frac{3}{2}}} \Phi \left\{ t_0'' \frac{2U_c}{(gb)^{\frac{1}{2}}} \left(\frac{3T_{2,1}}{T_{3,1}} \right)^{\frac{3}{2}} \right\}. \tag{5.8}$$

It will be observed that (5.6) and (5.7) differ from their counterparts (4.7) and (4.8) for laminar model B only through the inclusion of t_0'', which is directly proportional to the curvature of the velocity profile on the tube axis. With a parabolic profile $t(\eta) = \frac{1}{2}\eta^2 - 1$, and $t_0'' = 1$. We may anticipate that t_0'' will reduce with increasing flow Reynolds number: expressions for t_0'' will now be derived from published relationships for turbulent flow.

5.2.1. *Velocity profiles.* Dimensional arguments about the nature of the flow near the tube axis lead to the velocity defect law

$$(U_c - u)/u^* = \phi(\eta), \tag{5.9}$$

where the friction velocity is $u^* = (\tau_w/\rho)^{\frac{1}{2}} = \bar{U}(\frac{1}{2}f)^{\frac{1}{2}}$, τ_w is the shear stress on the tube wall and f the friction factor, for which we use the expression†

$$f^{-\frac{1}{2}} = 3{\cdot}5 \log Re - 2{\cdot}6. \tag{5.10}$$

Equation (5.10) gives an excellent description of the universal resistance law for smooth pipes for $Re = \rho \bar{U} D/\mu$ up to 10^9 and has the advantage of being explicit in f.

t_0'' is obtained from the definition (5.5) of $t(\eta)$ and (5.9), which give

$$-u_0'' = 2U_c t_0'' = \lambda_2 u^*, \tag{5.11}$$

where λ_2 is a dimensionless constant evaluated from $\phi(\eta)$. Using the velocity defect law at the radius where the local and mean velocities are equal, the law being valid over virtually the whole tube, gives the relation

$$U_c = \bar{U} + \lambda_1 u^*, \tag{5.12}$$

where λ_1 is dimensionless and is evaluated from $\phi(\eta)$. Combining (5.11) and (5.12) gives

$$t_0'' = (1 - \bar{U}/U_c)\, \lambda_2/2\lambda_1. \tag{5.13}$$

† 'log' denotes '$\log_{10}$' in this paper.

Several forms have been suggested for $\phi(\eta)$. Reichardt's (1951) theory, which describes experimental velocity profiles very well, expressed the eddy viscosity as a polynomial to give

$$(U_c - u)/u^* = 2{\cdot}5 \ln[(1+2\eta^2)/(1-\eta^2)]. \tag{5.14}$$

Integrating (5.14) across the tube gives $\lambda_1 = 3{\cdot}75 \ln 3 = 4{\cdot}12$, and differentiating (5.14) twice gives, from (5.11), $\lambda_2 = 15$; both values are in good agreement with Townsend's (1976) and Hinze's (1976) analyses of published data. For small η, (5.14) has the parabolic form

$$u = U_c - 7{\cdot}5u^*\eta^2, \tag{5.15}$$

showing that Reichardt's profile has zero velocity gradient on the tube axis; this parabolic constituent is the dominant feature of turbulent velocity profiles over a large region of the flow (de Moraes 1977). Figure 3(*b*) compares Reichardt's profile with Pai's (1957) equation

$$u = U_c[1 - \gamma\eta^2 - (1-\gamma)\eta^{2n}], \tag{5.16}$$

where γ and n may be determined by comparing (5.16) with (5.9). Large values of n are found to be necessary if turbulent data are to be described adequately, for example $n = 33{\cdot}5$ when $Re = 10^4$, and as a result the influence of the term η^{2n} in (5.16) is confined to the neighbourhood of the wall. We observe then that the exact solution of (2.1) used in the laminar theory represents a parabolic velocity profile with a superimposed irrotational perturbation while the simplified turbulent theory uses the same irrotational perturbation to disturb a turbulent profile whose dominant constituent is parabolic. In a sense the simplified theory may be viewed as an application of the exact solution for laminar flow over most of the tube, so that the manner in which the vorticity is convected around the slug seems likely to be well described by this approach, particularly near the tube axis.

5.2.2. *Evaluation and comparison with* (1.1). On using (5.10)–(5.14) together with the values for $T_{3,1}$ and $T_{2,1}$ from §4, and on rewriting in terms of D, (5.8) becomes

$$U_s = \overline{U}\left[\frac{\log Re + 0{\cdot}089}{\log Re - 0{\cdot}74}\right] + 0{\cdot}347(gD)^{\frac{1}{2}}\,\Phi\left\{\frac{\overline{U}}{(gD)^{\frac{1}{2}}}\,\frac{1{\cdot}81}{\log Re - 0{\cdot}74}\right\}. \tag{5.17}$$

The coefficient of $\overline{U}$ in (5.17) simply expresses the dependence of $U_c/\overline{U}$ on Re. Since $Re = (\overline{U}/(gD)^{\frac{1}{2}})(g^{\frac{1}{2}}D^{\frac{3}{2}}\rho/\mu)$, (5.17) may be regarded as a relationship between $U_s/(gD)^{\frac{1}{2}}$ and $\overline{U}/(gD)^{\frac{1}{2}}$ for a given value of $N_f = g^{\frac{1}{2}}D^{\frac{3}{2}}\rho/\mu$.

Figure 4 shows the form of (5.17) for $N_f = 12000$, the value appropriate to the experiments of Nicklin *et al.* (1962). The form is very nearly, but not quite, linear. Thus with the coefficients C_1 and C_2 suitably chosen, (1.1) can provide a good description of (5.17) but values for these coefficients could differ slightly depending on (i) the range of $\overline{U}/(gD)^{\frac{1}{2}}$ over which (1.1) and (5.17) are fitted to each other, (ii) the degree of inaccuracy in the representation considered acceptable, and (iii) the value of N_f. These factors may account for the differences in experimental values commented upon by Nobel (1972). For values of $\overline{U}/(gD)^{\frac{1}{2}}$ ranging from 0·6 to 4·9, i.e. for $Re > 8000$, Nicklin *et al.* (1962) found

$$U_s = 1{\cdot}2\overline{U} + 0{\cdot}35(gD)^{\frac{1}{2}}. \tag{5.18}$$

They observed that the coefficient 1·2 is close to the ratio $U_c/\overline{U} = 1{\cdot}22$ obtained from a one-seventh power-law profile. The slug velocity in stagnant liquid, $U_{s0} = 0{\cdot}35(gD)^{\frac{1}{2}}$,

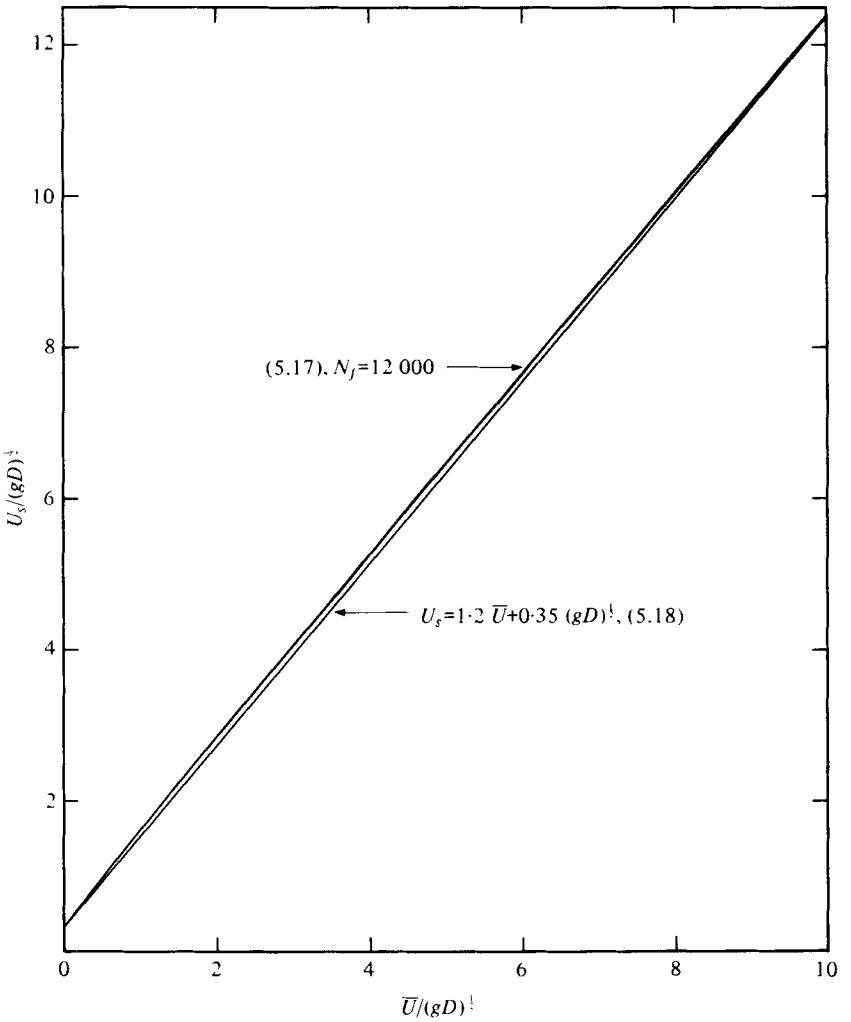

FIGURE 4. Slug velocity U_s as a function of flow velocity $\overline{U}$ from (*a*) the full solution for turbulent profiles, (5.17); (*b*) solution of Nicklin *et al.*, (5.18); for their data, $N_f = 12000$.

is the best available experimental value (Stewart & Davidson 1967). Figure 4 shows excellent agreement between (5.17) and (5.18) and thus confirms the simple interpretation given by Nicklin *et al.* that the slug velocity is the sum of the liquid velocity on the tube centre-line and the characteristic velocity of the slug in stagnant liquid.

Figure 5 shows the variation of $(U_s - U_{s0})/\overline{U}$ with $\overline{U}/(gD)^{\frac{1}{2}}$ obtained from the full solution (5.17), again with $N_f = 12000$ and the asymptotes of (5.17) from the expansions for Φ in (3.11) and (3.12). The two asymptotes intersect at $\overline{U}/(gD)^{\frac{1}{2}} = 2$ and together provide excellent descriptions of the full solution over the complete range of $\overline{U}/(gD)^{\frac{1}{2}}$. Thus, for $\overline{U}/(gD)^{\frac{1}{2}} < 2$

$$U_s = \overline{U}\left[\frac{\log Re + 0{\cdot}21}{\log Re - 0{\cdot}74}\right] + 0{\cdot}347(gD)^{\frac{1}{2}}, \tag{5.19}$$

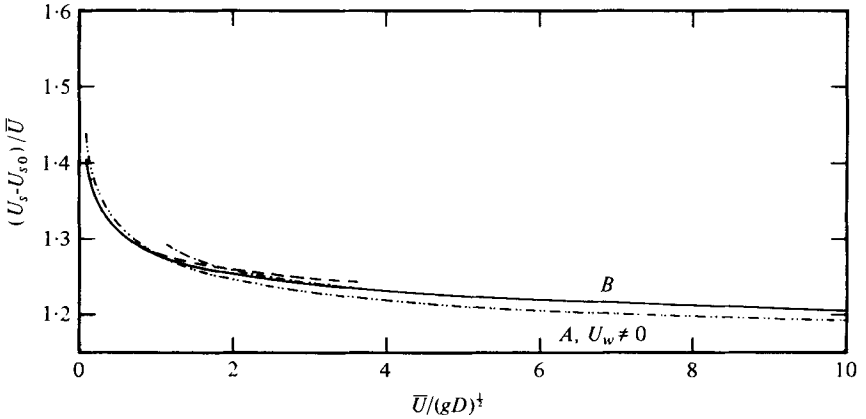

FIGURE 5. Results for turbulent models A and B, with $N_f = 12000$.

Model	Line	Equations
A	–·–·	(5.2), (5.3), (5.4) and (5.12), $U_w \neq 0$
B	——	(5.17)
	– – –	(5.19), asymptote to model B for $\overline{U}/(gD)^{\frac{1}{2}} < 2$
	–·–	(5.20), asymptote to model B for $\overline{U}/(gD)^{\frac{1}{2}} > 2$

while for $\overline{U}/(gD)^{\frac{1}{2}} > 2$

$$U_s = \overline{U}\left[\frac{\log Re + 0{\cdot}089}{\log Re - 0{\cdot}74}\right] + (gD)^{\frac{1}{2}}\left[\left(\frac{\overline{U}}{(gD)^{\frac{1}{2}}}\frac{0{\cdot}083}{\log Re - 0{\cdot}74}\right)^{\frac{1}{3}} + \frac{1}{3}\left(\frac{\overline{U}}{(gD)^{\frac{1}{2}}}\frac{5{\cdot}84}{\log Re - 0{\cdot}74}\right)^{-\frac{1}{3}}\right]. \tag{5.20}$$

When compared with (5.17), (5.19) shows that, for the turbulent profile as for the laminar, there is a slight enhancement of the coefficient of $\overline{U}$ for values of $\overline{U}/(gD)^{\frac{1}{2}} < 2$; but the effect is smaller than for the laminar theory, the maximum increase in C_1 being only about 3 % for $Re \simeq 4 \times 10^3$. Equation (5.19) gives the dependence of C_1 on Re for this low range of $\overline{U}/(gD)^{\frac{1}{2}}$. For $\overline{U}/(gD)^{\frac{1}{2}} > 2$, (5.20) describes the variations in C_2 with $\overline{U}/(gD)^{\frac{1}{2}}$, although at high values of $\overline{U}/(gD)^{\frac{1}{2}}$ the first term in (5.20) is dominant; that term is moreover identically equal to U_c. We stress again that, while (5.19) and (5.20) are useful for interpretative purposes, the full solution in (5.17) is easily evaluated.

Figure 5 also shows the results for turbulent model A based on the exact solution of (2.1) for a particular value of U_w determined by choosing α to satisfy (5.4) and (5.12) so as to match the velocity profile with known turbulent profiles over the central part of the tube. The fact that its results are similar to those obtained for the simplified theory of turbulent model B provides further support for that approach.

6. Comparison of theory and experiment

Since there are few published data on inertia-controlled slugs with laminar flow of the liquid, we carried out experiments to measure the slug velocity and the radius of curvature at the nose in the laminar region $0 < Re < 2100$ and the transition region $2100 < Re < 4000$.

There were two requirements, namely (i) that the liquid flow should give the above

ranges of Reynolds numbers, and (ii) that the slug motion should be inertia-controlled, which for stagnant liquid, as noted in §1, implies $N_f > 300$ and $Eo > 100$. These conditions were met by using a mixture of 48% by weight glycerol with water in a tube of diameter 51·4 mm. For this mixture, $N_f = 7\,600$, $Eo \simeq 420$ and the ranges of liquid velocities and Reynolds numbers were $0 < \bar{U} < 37$ cm/s and $0 < Re < 4000$; for water the corresponding values were $N_f = 36\,500$, $Eo = 357$, $0 < \bar{U} < 40$ cm/s and $0 < Re < 20\,700$.

The tube was 4 m long. The liquid entered at the bottom through a calming section 30 cm long packed with 5 mm glass ballotini. Slugs of air were injected just above the calming section; 2·5 m further up, the slug velocity was obtained from an electronic measurement of the interval between the times at which a slug activated two impedance probes separated by a distance of 30 cm. The results were checked in a few cases by ciné photography of a rising slug.

For each choice of liquid velocity, 10 readings of the slug velocity were usually taken, but if the data showed some variability, as for very low liquid velocities, 20 or 30 readings were taken. The range of standard deviations was from about 0·7% to less than 3% for high and low liquid velocities respectively.

With stagnant liquid, the standard deviation was very small, 0·16%, and the measured slug velocity, 24·63 cm/s, was in excellent agreement with (4.11), from which, with $\bar{U} = 0$, $U_{s0} = 24{\cdot}64$ cm/s. A typical middle range reading for the glycerol–water mixture was $\bar{U} = 10{\cdot}09 \pm 0{\cdot}03$ cm/s, $U_s = 43{\cdot}49 \pm 0{\cdot}19$ cm/s, $C_1 = 1{\cdot}87 \pm 0{\cdot}03$ and $Re = 1080$.

The radius of curvature a of the nose of a slug was measured by tracing a projected photograph. For each liquid velocity, three individual slugs were photographed. The refraction effect was minimized by encasing a section of the tube in a square Perspex box filled with glycerol. Figure 2 shows that the change of slug shape predicted by the theory is reflected in the measurements: the radius of curvature at the nose is reduced by liquid flow, the data being in reasonable agreement with model *B*.

Experimental measurements of the slug velocity are plotted in figure 6 as the dimensionless slug velocity $U_s/(gD)^{\frac{1}{2}}$ *vs.* the dimensionless liquid velocity $\bar{U}/(gD)^{\frac{1}{2}}$. Theory and experiment for the laminar case are seen to agree well when the parabolic profile is established experimentally, i.e. at low velocities in the glycerol–water mixture. As a laminar regime occurs for $Re < 2100$ and since $Re = N_f \bar{U}/(gD)^{\frac{1}{2}}$, we should expect that data obtained in this regime would follow (4.11) up to (i)

$$\bar{U}/(gD)^{\frac{1}{2}} < 0{\cdot}28$$

with a 48% glycerol–water mixture, for which $N_f = 7600$, and (ii) up to

$$\bar{U}/(gD)^{\frac{1}{2}} < 0{\cdot}06$$

with water, for which $N_f = 36\,500$. However, figure 6 shows that the experimental points deviate from (4.11) at values of $\bar{U}/(gD)^{\frac{1}{2}}$ lower than these expectations, owing to entrance effects, though the agreement is good when $\bar{U}/(gD)^{\frac{1}{2}} < 0{\cdot}1$. As described earlier, the liquid entered the tube through a calming section which produced a flat velocity profile. The ratio (entry length)/D for laminar flow in circular tubes is proportional to Re, the constant of proportionality being variously quoted as 0·08 (theoretical, White 1974) or 0·028 (experimental, Govier & Aziz 1972); it follows that

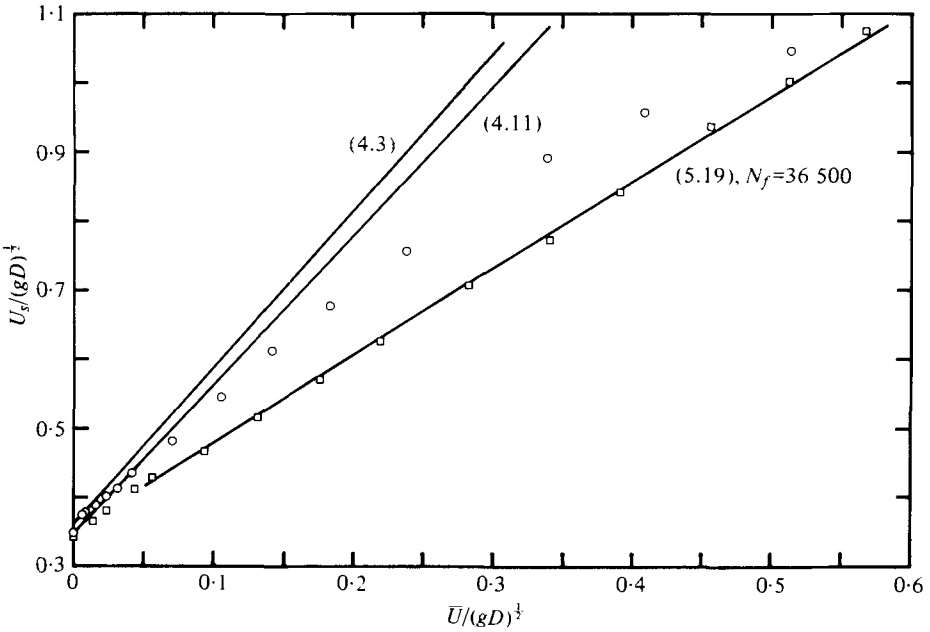

FIGURE 6. Dimensionless slug velocity *vs.* dimensionless liquid velocity. □, air/water; ○, air/48 % by weight glycerol–water.

measurements of slug velocity at 2·5 m above the liquid distributor allowed a full development of a laminar profile only at low Re. This explains why the laminar theory and experiment agree only at low liquid velocities in this apparatus.

In §2 it was noted that the slug motion is inertia-controlled provided $Re_s > 105$ and that the boundary layers are then expected to be thin. For flowing liquid, $Re_s > 105$ implies, using (4.12) and (5.17), that

$$(2{\cdot}16 \rightarrow 1)\,Re + 0{\cdot}35N_f > 105, \tag{6.1}$$

where $(2{\cdot}16 \rightarrow 1)$ implies a range of coefficients. There is the additional constraint $Eo > 100$ as for stagnant liquid. From (6.1) it follows that the slug is inertia-controlled for increasing viscosities as the liquid flow increases. In particular, if the upward flow is turbulent, it is sufficient that $Eo > 100$ for (5.17) to be applicable.

Provided these constraints are satisfied, the slug velocity is independent of viscosity for laminar flow. But for turbulent flow, owing to the presence of Re in (5.17), a plot like figure 6 would give a family of lines with N_f as a parameter.

Figure 6 shows excellent agreement between slug velocity data for turbulent flow and (5.19), which is an asymptote of (5.17). Nicklin *et al.* (1962) obtained a good fit with (5.18) for data over a much larger range of Re than that shown in figure 6. The acceptance of (5.18) in the literature, and the excellent agreement between (5.17) and (5.18) shown in figure 4, therefore confirm an agreement between theory and experiment for essentially all liquid velocities of common interest.

One of us (F.F. de M.) would like to thank the University of Maringá, Brazil, and the British Council for support during the course of this work.

REFERENCES

BATCHELOR, G. K. 1967 *An Introduction to Fluid Dynamics*, pp. 507–593, 475. Cambridge University Press.

BEHRINGER, P. 1936 *Z. Geo. Kalte. Ind.* **43** (3), 55–58.

COLLINS, R. 1966 *J. Fluid Mech.* **25**, 469–480.

COLLINS, R. 1967 *J. Fluid Mech.* **28**, 97–112.

COLLINS, R. 1968 Gas bubbles in liquids and in fluidized beds. Ph.D. thesis, University of London.

COLLINS, R. & HOATH, M. T. 1973 *J. Fluid Mech.* **57**, 515–527.

DAVIES, R. M. & TAYLOR, G. I. 1950 *Proc. Roy. Soc.* A **200**, 375.

DUMITRESCU, D. T. 1943 *Z. angew. Math. Mech.* **23**, 139–149 (English trans. obtainable from Library (translations), Bldg 465, AERE, Harwell).

GOVIER, G. W. & AZIZ, K. 1972 *The Flow of Complex Mixtures in Pipes*, pp. 388–414, 142. Van Nostrand.

GRIFFITH, P. & WALLIS, G. B. 1961 *J. Heat Transfer* **83**, 307–320.

HAWTHORNE, W. R. 1967 In *Fluid Mechanics of Internal Flow* (ed. G. Sovran), pp. 239–269. Elsevier.

HINZE, J. O. 1976 *Turbulence*, p. 733. McGraw-Hill.

LAI, W. 1964 *J. Fluid Mech.* **18**, 587–594.

LAMB, H. 1932 *Hydrodynamics*, p. 245. Cambridge University Press.

LAYZER, D. 1955 *Astrophys. J.* **122**, 1–12.

MORAES, F. F. DE 1977 Gas slugs in liquids and three-phase fluidisation. Ph.D. dissertation, University of Cambridge.

NICKLIN, D. J., WILKES, J. O. & DAVIDSON, J. F. 1962 *Trans. Inst. Chem. Engrs Lond.* **40**, 61–68.

NICOLITSAS, A. J. & MURGATROYD, W. 1968 *Chem. Engng Sci.* **23**, 934–936.

NOBEL, L. 1972 *The Slug Flow Equation.* Commission of the European Communities, Joint Nuclear Research Centre – Ispra Establishment (Italy), Technology, Luxembourg, EUR. 4811 e.

PAI, S. I. 1957 *Viscous Flow Theory*, vol. 2, p. 43. Van Nostrand.

REICHARDT, H. 1951 *Z. angew. Math. Mech.* **31**, 208–219.

STEWART, P. S. B. & DAVIDSON, J. F. 1967 *Powder Tech.* **1**, 61–80.

TOWNSEND, A. A. 1976 *The Structure of Turbulent Shear Flow*, 2nd edn, p. 150. Cambridge University Press.

WALLIS, G. B. 1969 *One Dimensional Two-Phase Flow*, pp. 282–314. McGraw-Hill.

WHITE, E. T. & BEARDMORE, R. H. 1962 *Chem. Engng Sci.* **17**, 351–361.

WHITE, F. M. 1974 *Viscous Fluid Flow*, p. 338. McGraw-Hill.

ZUBER, N. & FINDLAY, J. A. 1965 *J. Heat Transfer* **87**, 453–468.